Guocan Jiang, Jin Wang, Nuoya Li, René Hübner, Maximilian Georgi, Bin Cai, Zhengquan Li, Vladimir Lesnyak, Nikolai Gaponik, Alexander Eychmüller

Self-Supported Three-Dimensional Quantum Dot Aerogels as a Promising Photocatalyst for CO_2 Reduction

Erstveröffentlichung in / First published in:

Chemistry of Materials. 2022, 34 (6), S. S. 2687–2695. ACS Publications. ISSN 1520-5002.

DOI: https://doi.org/10.1021/acs.chemmater.1c04028

Self-Supported Three-Dimensional Quantum Dot Aerogels as A Promising Photocatalyst for CO_2 Reduction

*Guocan Jiang,[1] Jin Wang,[*2] Nuoya Li,[2] René Hübner,[3] Maximilian Georgi,[1] Bin Cai,[4] Zhengquan Li,[2] Vladimir Lesnyak,[1] Nikolai Gaponik,[*1] and Alexander Eychmüller[1]*

[1] Physical Chemistry, Technische Universität Dresden, Zellescher Weg 19, 01069 Dresden, Germany.

[2] Key Laboratory of the Ministry of Education for Advanced Catalysis Materials, Zhejiang Normal University Jinhua, 321004 Zhejiang, P.R. China.

[3] Helmholtz-Zentrum Dresden-Rossendorf, Institute of Ion Beam Physics and Materials Research, Bautzner Landstrasse 400, 01328 Dresden, Germany.

[4] School of Chemistry and Chemical Engineering, Shandong University, Shanda South Road 27, Jinan 250100, P.R. China.

*Correspondence:

wangjin@zjnu.edu.cn (J.W.)

nikolai.gaponik@tu-dresden.de (N.G.)

ABSTRACT

Armed with merits of the quantum dots (QDs) (e.g., high molar extinction coefficient, strong visible light absorption, large specific surface area, and abundant functional surface active sites) and aerogels (e.g., self-supported architectures, porous network), semiconductor QD aerogels show great prospect in photocatalytic applications. However, typical gelation methods rely on oxidative treatments of QDs. Moreover, the rests of organic ligands (e.g., mercaptoacids) are still present on the surface of gels. Both these factors inhibit the activity of such photocatalysts, hampering their widespread use. Herein, we present a facile 3D assembly of II-VI semiconductor QDs capped with inorganic $(NH_4)_2S$ ligands into aerogels by using H_2O as a dispersion solvent. Without any sacrificial agents, the resulting CdSe QD aerogels achieve high CO generation rates of 15 μmol g^{-1} h^{-1} which is 12-fold higher than that of the pristine aggregated QD powders. Our work not only provides a facile strategy to fabricate QD aerogels, but also offers a platform for designing advanced aerogel-based photocatalysts.

INTRODUCTION

Sunlight-driven CO_2 reduction is a very appealing approach to simultaneously solve the problems of the fossil fuel induced crisis and global warming.[1-3] However, CO_2 reduction is difficult to achieve as it requires a large energy to break the C=O bond (~750 kJ/mol) and involves multi-electron reactions.[4,5] In addition, it remains a big challenge to efficiently capture CO_2 molecules from the atmosphere.[6] To reach this goal, it is urgent to design and develop a visible-light responsive semiconductor photocatalyst possessing among others the following characteristics: 1) sufficiently negative conduction band (CB) potential for CO_2 reduction, 2) ability for efficient charge separation and transfer, 3) strong CO_2 capture capacity, 4) abundant catalytic sites for specific reactions.

Quantum dots (QDs) are one of the most attractive semiconductors for photocatalysis due to their many excellent photoelectronic properties, including high molar extinction coefficients, tunable bandgaps, as well as abundant surface sites.[5,7-15] In recent years, various QDs (e.g., CdS, CdSe, $CuInS_2$, and $CsPbBr_3$) have been developed for photocatalytic CO_2 reduction, demonstrating the great potential of QD photocatalysts.[5,9,10,12,13,15-17] However, the colloidal QDs are usually capped with organic ligands, which may prevent the effective contact between the QDs and reactants (e.g., CO_2 and H_2O).[16,18,19] That is, the number of available catalytic sites on those QD surfaces is reduced due to the occupation by capping ligands. In addition, most of the reported QD photocatalytic systems are based on liquid-solid catalytic reactions, where the well-dispersed QDs are nearly isolated from each other and react with the substrates by random collisions.[5,11,16,18] As a result, these systems suffer from a low CO_2 adsorption capacity and charge transfer efficiency. The drawbacks mentioned above limit the wide application of colloidal QD photocatalysts.

Inspired by the three-dimensional (3D) network of leaves, various porous materials (e.g., covalent organic frameworks, metal-organic frameworks, and aerogels) with self-supporting architectures have been

constructed for photocatalysis.[20-22] Among them, aerogels based on QDs are promising candidates for photocatalytic CO_2 reduction because the aerogel structure can endow them with high porosity and strong gas adsorption.[23-27] In addition, the microporous structure of QD aerogels enhances the ability to capture light and increases mass transport efficiency.[26] Importantly, the intimate contact between individual QDs can promote charge separation and transfer in QD aerogels.[28] Therefore, it appears to be an appealing endeavor to design and develop QD aerogels for photocatalytic CO_2 reduction. Although many QD aerogels have been successfully prepared during the last 15 years, their photocatalytic properties remain largely unexplored.

Herein, we present novel CdSe QD aerogels with 3D self-supported architecture for visible-light-driven CO_2 reduction. The QD aerogels were prepared by a facile self-assembly approach based on the destabilization of S^{2-}-capped colloidal QDs with H_2O as a dispersion solvent. Afterwards, the transition metal cations (e.g., Fe^{2+}, Co^{2+}, and Ni^{2+}) as co-catalysts were immobilized on the QD gel surface by an immersion deposition. The self-supported porous structure of the aerogel renders the QDs with a strong CO_2 capture capacity and enhances their light-harvesting ability. Finally, the QD aerogels exhibit superior photocatalytic performance in gas-phase CO_2 reduction at ambient pressure. Without any sacrificial agents, the yield of CO over the CdSe QD aerogel reached approx. 15 mol g^{-1} h^{-1}, which is much higher than that of the pristine aggregated QD powders. Further investigations shed light on a mechanism for the significant enhancement of photocatalytic activity. Our work provides a platform for designing various QD aerogels and broadens their applications in solar-to-fuel conversion.

RESULTS AND DISCUSSION

The gelation process

Oxidative ligand etching and ion coupling are two main methods to destabilize colloidal QDs for preparing aerogels.[29-35] However, these methods may easily destroy the QDs and introduce undesired impurities during the gelation, which would be detrimental for their further applications. To avoid this, we developed a facile gelation strategy toward QD aerogels. As a proof of concept, CdSe QDs were selected as the specimen, as they possess suitable CB potentials for CO_2 reduction and are strong harvesters with tunable absorption covering nearly entire visible-light range. The gelation process and proposed scheme are illustrated in **Figure 1a** and **1b**, respectively. Specifically, oleic acid (OA)-capped CdSe (simplified as CdSe-OA hereafter) QDs were firstly synthesized by a heating-up method (see details in the Supporting Information (SI)).[36] The as-prepared QDs have a narrow size distribution with an average diameter of ca. 3.2 ± 0.4 nm (**Figure 1c** and **Figure S1**). Afterwards, the long-chain OA was exchanged with $(NH_4)_2S$ to obtain QDs dispersed in N-methylformamide (NMF), which refer as CdSe-S hereafter.[37] The first absorption peak is red-shifted from 518 nm to 532 nm (**Figure S2**). The redshift can indicate the growth of a CdS shell resulting in a bigger particle size and a lower carrier confinement.[14,38] Similar redshift also appears in the emission spectrum accompanied by a significant decrease in fluorescence intensity (**Figure S3**). This quenching is typically observed for the incoming $(NH_4)_2S$ ligand, which can act as an additional hole trap.[39] Compared to the CdSe-OA QDs, the CdSe-S QDs have a lower colloidal stability and are inclined to gelation. The partial aggregation of the CdSe-S QDs dispersed in NMF can be seen in **Figure 1d** and **Figure S4**. When the solvent of the CdSe-S QDs was changed from NMF to H_2O (see details in the SI) and allowed to age for two days, the CdSe-S QDs spontaneously assembled into gels (**IV** of **Figure 1a** and **Figure 1e**). This gelation process was also monitored by dynamic light scattering (DLS). As shown in **Figure S4**, the average size of dispersed species increased from the nanometer to the micrometer range, which is typical for the early stages of gelation.[40,41] Finally, the CdSe-S gels were supercritically dried to obtain CdSe-S aerogels with a 3D open porous structure (**Figure 1f**). High-resolution transmission

electron microscopy (HRTEM) image demonstrates that the resulting CdSe-S aerogels are made of well-connected CdSe-S QDs retaining their crystallinity (**Figure S5**).

We further gain an insight into the gelation mechanism. It is well known that controlled destabilization is necessary for the preparation of QD-based gels.[42,43] The following factors trigger the destabilization during our gelation process. The ligand exchange removes the long-chain OA, which brings the individual QDs in an intimate contact. In addition, this ligand exchange turns the sterically stabilized QDs into electrostatically stabilized ones. When the CdSe-S QDs were dispersed in H_2O, the balance between electrostatic repulsion and attractive forces between the QDs (including van der Waals and dipole-dipole interactions) changed significantly because of the smaller dielectric constant of H_2O ($\varepsilon = 78.5$) relative to NMF ($\varepsilon = 180$).[44,45] Under these conditions, the electrical double layer around individual nanoparticles becomes smaller thus increasing the probability for nanoparticles to approach each other. The reduced colloidal stability is reflected by the zeta-potential (ζ) values of the corresponding samples: -15 mV in H_2O vs. -35 mV in NMF. It is important to note that the freshly prepared hydrogel can be redispersed in NMF forming quasi-stable sol (**Figure S6a**). This partial reversibility is even better seen from the evolution of the zeta-potential values of the CdSe-S solution in NMF during the titration with water (**Figure S6b**). The zeta-potential is reduced upon increasing the volume fraction of water and this trend can be reverted as soon as more NMF is added to the mixture. Another destabilizing factor induced by the presence of water can be the protonation of the surface S^{2-} ligands, which is, however, less probable as the gelation takes place at pH values above 8. Based on our general experience in the QD gelation, the method introduced in the present work is relatively less destructive, does not demand additional linkers [32,33]oxidizers[31,35,46] or depletants[47] and allows for preserving the intrinsic properties of the QDs.[48,49] Furthermore, since S^{2-} can stabilize a variety of semiconductor QDs and most of the noble metal nanoparticles,[37] our gelation method is quite versatile. To demonstrate this versatility, we have also

successfully prepared an aerogel from CdS QDs and noble metal aerogels of Au and Pd, which will be reported elsewhere.

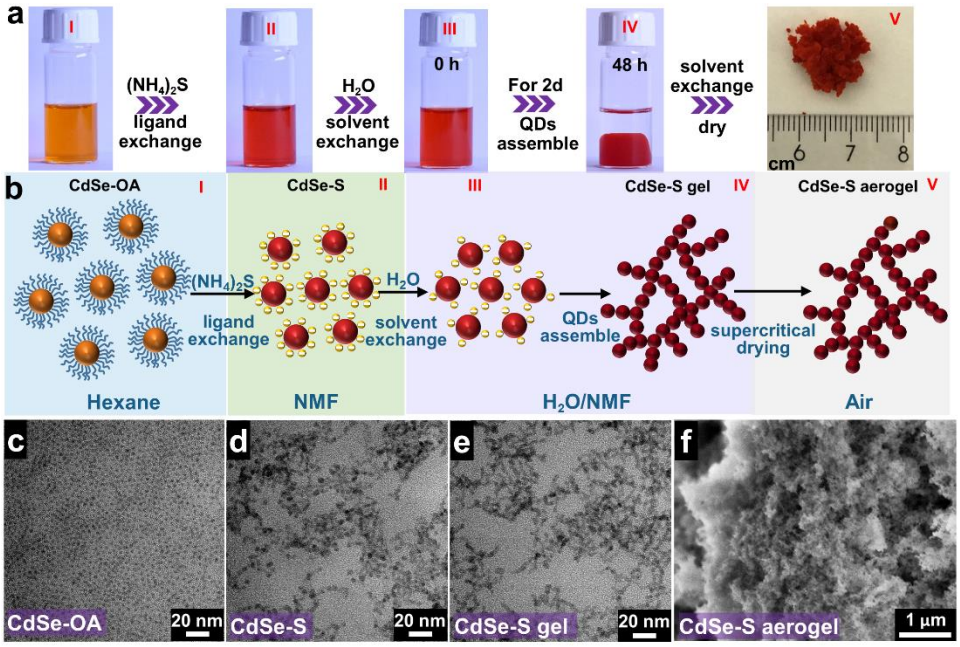

Figure 1. Overall gelation process of CdSe-S QDs. (a) The process of preparing the CdSe-S aerogel. (b) Schematic illustration of the proposed gelation mechanism. TEM images of (c) the initial CdSe-OA QDs in hexane, (d) CdSe-S QDs in NMF, (e) CdSe-S gel. (f) SEM image of CdSe-S aerogel.

Characterization of the QD aerogels

The as-prepared CdSe-OA QDs show a zinc-blende crystal structure (**Figure 2a**). After ligand exchange, the main diffraction peaks of the CdSe-S QDs shift slightly toward larger angles, indicating a contraction of the lattice. This is due to a partial incorporation of ligand S^{2-} ions into the lattice forming a thin CdS layer on the CdSe surface.[7,50] Furthermore, the crystal structure of the CdSe-S QDs does not change during gelation and supercritical drying. In the Fourier-transform infrared (FTIR) spectra (**Figure 2b**), some typical bands centered at 2852, 2925, and 1466 cm^{-1}, which can be assigned to hydrocarbon species, disappeared to a large extent after the ligand exchange and completely after the gelation and drying, thus

proving an efficient elimination of the OA molecules from the QD surface. Furthermore, the thermogravimetric analysis (TGA) results indicate that the CdSe-S aerogel lost only ca. 5% of its weight after heating up to 500 °C (**Figure 2c** and **Figure S7**). This behavior is another indirect evidence of the fact that there is almost no ligands associated with the aerogel surface. The as-prepared aerogel was further characterized by high-angle annular dark-field scanning transmission electron microscopy (HAADF-STEM) imaging combined with element mapping based on energy-dispersive X-ray spectroscopy (EDX) to determine its elemental composition. As shown in **Figure 2d-g**, the QD aerogel exhibits a well-connected network structure, with Cd, Se, and S distributed in the network. Summarizing the above results, we can conclude that the CdSe-S aerogels are composed of interconnected highly crystalline CdSe-S QDs with a "naked" (e.g. free of organic ligands) surface, which is very beneficial for its application in photocatalysis.[18,27]

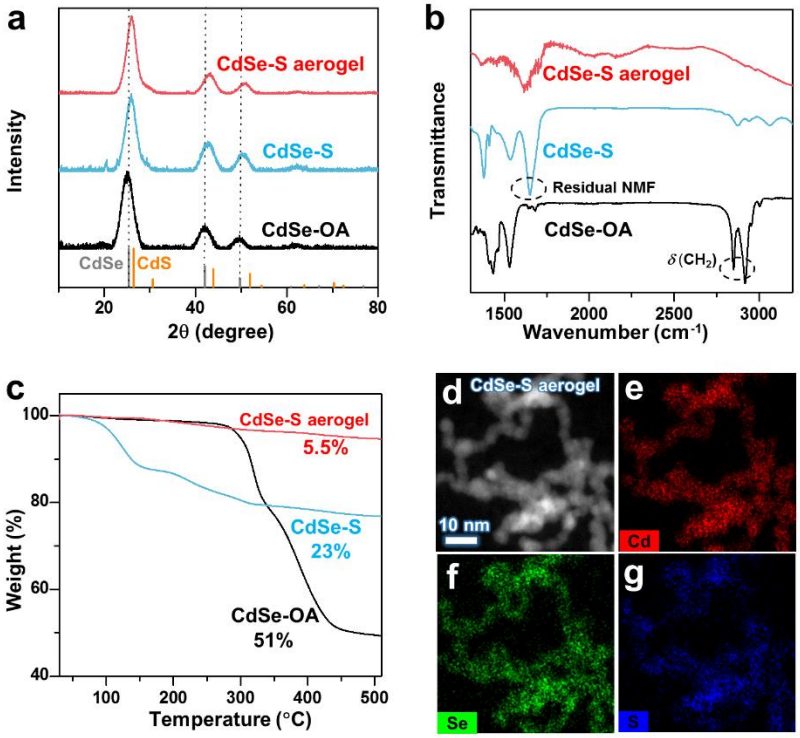

Figure 2. Characterization of CdSe-S aerogel. (a) XRD patterns of CdSe-OA QDs, CdSe-S QDs, and the CdSe-S aerogel. The reference diffraction peaks of CdSe and CdS are taken from C19-191 and PDF#65-2887, respectively. (b) FT-IR spectra of CdSe-OA QDs, CdSe-S QDs and the CdSe-S aerogel. (c) TGA of CdSe-OA QDs, CdSe-S QDs, and the CdSe-S aerogel. (d) Overview HAADF-STEM image of the CdSe-S aerogel and corresponding element maps based on EDX analysis: (e) Cd, (f) Se, and (g) S.

Performance of CdSe-S aerogels in photoreduction of CO_2

The photocatalytic activity of various catalysts based on CdSe-S QDs was assessed in the presence of CO_2 and H_2O (see **Figure S8**). As shown in **Figure 3a** and **Figure S9**, the pristine CdSe-S QD powders exhibit low catalytic activity toward CO_2 reduction, mainly due to the lower specific surface area (**Figure S10**).[35] In contrast, the CdSe-S aerogels display a much more enhanced catalytic activity, as they possess a self-supported porous structure with strong CO_2 and light capture capacity.[23,26] Nonetheless, most of the photoexcited charge carriers in the CdSe-S QD aerogels were wasted due to the lack of efficient catalytic sites to capture them. Therefore, transition metal cations (e.g., Ni^{2+}, Fe^{2+}, and Co^{2+}) were introduced to

our photocatalytic system as active catalytic centres. According to the hard and soft acid and base theory,[51] these metal cations have a strong affinity to sulfide species on the QD surface. As displayed in **Figure 3a**, after immobilizing Ni^{2+} cations onto the QD surface (see details in the SI), the resulting aerogels (simplified as CdSe-S/Ni hereafter) exhibit a significantly enhanced catalytic activity with respect to the pristine CdSe-S aerogels. Furthermore, the catalytic activity of the CdSe-S/Ni aerogels can easily be tuned by changing the amount of $NiCl_2$ added in the CdSe-S aerogels. With the increase of $NiCl_2$ content from 0.25 to 2 mol% relative to Se, the catalytic activity of the CdSe-S/Ni aerogels shows a volcano tendency. The CdSe-S/$Ni_{(3)}$ aerogel exhibits a maximal CO generation rate of 15 μmol g^{-1} h^{-1} with nearly 100% selectivity, which is 12-fold higher than that of the pristine CdSe-S QD powders. We note that the photocatalytic performance of our QDs-based aerogels is superior to many reported aerogel materials, as listed in **Table S1**. At the same time, the reported values cannot be correctly compared with the results of the widely investigated solution-based CO_2 reduction, as in this case the reactions are drastically accelerated due to the application of the sacrificial agents (hole scavengers). The improved photocatalytic activity is attributed to the self-supported porous structure and effective immobilization of Ni^{2+} cations on the QDs aerogels.[13,15] The excessive Ni^{2+} cations will become recombination centers and lead to a decrease in photocatalytic activity.[13,15] To assure that aerogel structure contributes on its own into the process, we treated the non-gelated CdSe-S powders with the same optimal amount of Ni. The catalytic activity of this kind of a reference sample was at least 3 times lower than that of the CdSe-S/Ni aerogels (**Figure S9**). This result further indicates that the unique architecture of the CdSe-S aerogel facilitates the charge transfer and CO_2 adsorption for CO_2 reduction. After that, we evaluated the durability of the CdSe-S/Ni photocatalyst. The photocatalytic activity still maintained about 90% of the original performance after 18 cycles (2 h per cycle) of the photocatalytic reaction (**Figure 3b**). Isotope labeling experiments were adopted to trace the source of the reaction product CO. When $^{13}CO_2$ was used as the

feedstock, a signal with m/z value of 29 assigned to ^{13}CO was detected (**Figure 3c**). In addition, the oxygen (O_2) evolution for the CdSe-S/$Ni_{(3)}$ aerogel was monitored during the CO_2 reduction (**Figure S11**). The O_2 generation rate is nearly a half of the rate for CO_2 reduction. This result indicates that the charge consumption at both sides of the CdSe-S/Ni photocatalyst is well balanced. Control experiments further confirmed that the generated CO originates from the photocatalytic reduction of CO_2 (**Figure S12**). To investigate whether our catalytic system is universal, other transition metal cations, such as Fe^{2+} and Co^{2+}, were also immobilized on CdSe-S QD aerogels, which also exhibited good catalytic activity toward CO_2 reduction (**Figure 3d**).

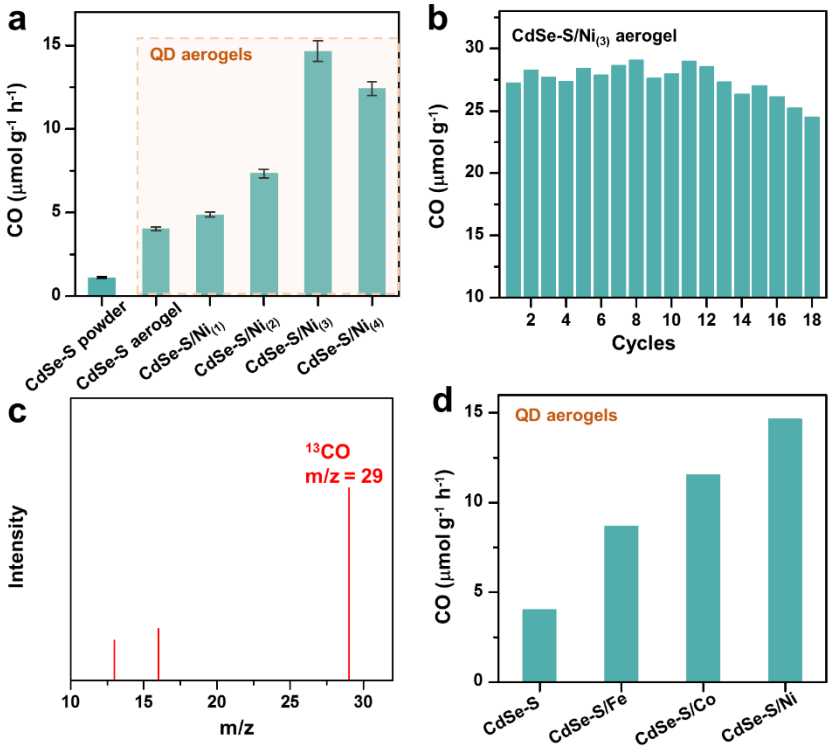

Figure 3. **Performance of CdSe-S QD aerogel samples in photoreduction of CO_2.** (a) Average production rates of CO by CdSe-S powders and aerogels with various Ni amounts (abbreviated as CdSe-S/$Ni_{(x)}$). (b) Photocatalytic durability test with eighteen 2 h cycles. (c) Mass spectrum showing ^{13}CO (m/z = 29) produced by CdSe-S/$Ni_{(3)}$ aerogel in the $^{13}CO_2$ photoreduction. (d) Average production rates of CO from CdSe-S aerogels with different metal cations immobilized on their surfaces. Conditions unless stated otherwise: 100 mW cm^{-2}, $\lambda > 400$ nm, 4 h, 25 °C.

Mechanism of enhanced photocatalytic performance

Subsequently, we tried to clarify the mechanism of photocatalytic CO_2 reduction on CdSe-S/Ni aerogels. It is well known that the QDs have large specific surface area, while the presence of native organic ligands reduces the available surface area for catalysis. Compared to the pristine colloidal CdSe-OA QDs, the CdSe-S QDs have a nearly naked surface. Therefore, the 3D self-supported aerogels consisting of CdSe-S QDs should theoretically have a larger available specific surface area. As shown in **Figure 4a**, the CdSe-S QD aerogels display a huge specific surface area of 272 m^2/g with a broad pore size distribution (**Figure 4b** and **Table S2**), the former being higher than most reported results summarized in **Table S3**. The specific surface area of the corresponding CdSe-S powder is only 62 m^2/g (**Figure 4a**). The immobilization of Ni cations on QD aerogels has a negligible influence on their specific surface area (**Figure S13**), implying that the architecture of the QD aerogels is well preserved. Moreover, the 3D self-supported porous structure of the CdSe-S/Ni aerogels makes them ideal candidates for gas-solid photocatalysis.[52,53] X-ray photoelectron spectroscopy (XPS) spectra revealed that the Ni species mainly exist in the Ni^{2+} oxidation state (**Figure S14**) and that there is a strong interaction between Ni^{2+} and the CdSe-S QDs (**Figure S15**). The presence of Ni in the CdSe-S/$Ni_{(3)}$ aerogel has also been proven in the EDX sum spectra obtained from STEM-based spectrum imaging analysis, resulting in an element composition of $Cd_{1.92}Ni_{0.012}Se_{1.00}S_{0.89}$ (**Figure S16**). The Ni distribution maps themselves do not show a discernible element signal implying that there is no significant Ni agglomeration, which makes us assume that the low nickel content is rather uniformly distributed on the aerogel network (**Figure S17**). Further investigations revealed that the presence of Ni does not affect the absorption spectrum of the CdSe-S aerogels (**Figure S18**), suggesting that the Ni^{2+} species mainly act as catalytic sites to capture photoexcited electrons for catalytic reactions. Many published studies have confirmed that the QDs assembled into aerogels are more favorable to the spatial separation of photoexcited electron-hole pairs compared to

isolated QDs.[28,54] The photogenerated carriers are easy to transfer between neighboring QDs after assembly. At the same time, the majority of the QDs in the aerogel offer the accessible surface and separated carriers can reach catalytic sites with a higher probability.[28,55] The higher possibility of a charge carrier separation may also be indirectly confirmed by the significantly quenched fluorescence of the QDs after their gelation. A more in-depth and complete study based on transient absorption spectroscopy of our photocatalytic system is in progress. We further adopted *in-operando* XPS to investigate the role of immobilized Ni^{2+} on the CdSe-S/Ni QD aerogels. Under light illumination, the binding energies assigned to Cd 3*d* in the CdSe-S/Ni aerogels shift to more positive values, implying a decreased electron density on CdSe (**Figure 4c**).[56] In addition, the binding energies assigned to S 2p display a positive shift, revealing a decreased electron density on S species (**Figure 4d**). The S^{2-} ions interact strongly with Cd^{2+} and Ni^{2+} and can serve as the bridge between CdSe and the co-catalyst (Ni^{2+}). We therefore infer that the photoexcited electrons in CdSe QDs can be transferred to Ni^{2+} cations through S^{2-} ions. The significantly enhanced photocurrent response in **Figure 4e** further demonstrates the efficient charge separation and transfer in the CdSe-S/Ni aerogel. On the basis of the above characterization results, we propose a possible photocatalytic mechanism for the CdSe-S/Ni QD aerogels, as illustrated in **Figure 4f**. Gaseous CO_2 and H_2O are firstly adsorbed at the porous CdSe-S QD aerogel surface. At the same time, under visible light irradiation, the nano-scale pores are expected to endow the QD aerogel with strong light harvesting by reflecting and scattering light.[26] The photoexcited carriers in the QDs swiftly transfer to their neighboring QDs, resulting in an efficient charge separation. Subsequently, the photogenerated electrons that are distributed in the entire QD aerogel are trapped by Ni^{2+} cations immobilized on the QDs surface. The adsorbed CO_2 and H^+ derived from the oxidation reaction of H_2O are eventually reduced to CO and H_2O by the electrons on the Ni^{2+} catalytic sites. At the same time, the generated holes oxidized H_2O into O_2 and H^+. Thus, H_2O participated in the photocatalytic CO_2 reduction, but was not consumed.

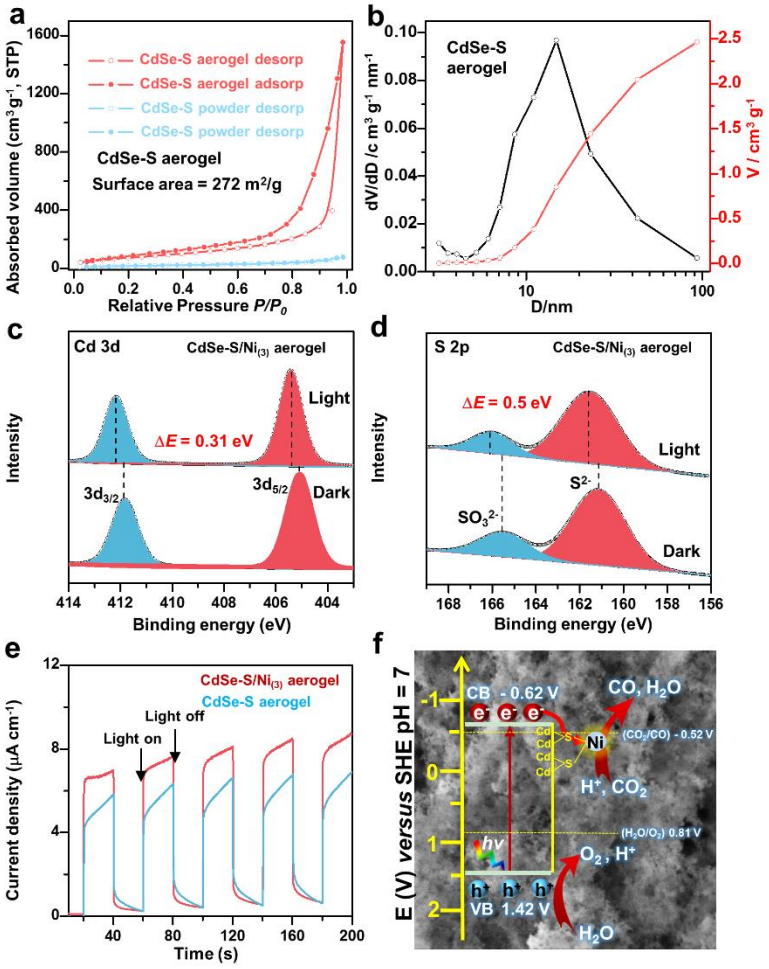

Figure 4. Photocatalytic mechanism of the CdSe-S/Ni aerogels. (a) N_2 physisorption isotherms of the CdSe-S aerogel and the powder. (b) Pore size distribution and pore volume in the CdSe-S aerogel. The detailed parameters are listed in **Table S2**. In operando high-resolution XPS for Cd 3d (c) and S 2p (d) spectra of CdSe-S/$Ni_{(3)}$ aerogel in the dark or under light irradiation. (e) I-t curves plotted at 0.2 V versus Ag/AgCl under light illumination (100 mW cm^{-2}). (f) Schematic representation of the CdSe-S/Ni aerogel photocatalytic system. The positions of energy bands are estimated from a combination of published data and experimental results (XPS) as described in the caption to **Figure S19**.

CONCLUSION

To sum up, we present a facile method to prepare QD aerogels for the photocatalytic CO_2 reduction. These QD aerogels exhibit high photocatalytic activity and selectivity toward CO_2 reduction. The improved photocatalytic performance of the QD aerogels mainly originates from three factors: 1) the self-supported porous structure of aerogel contributes to the light harvesting and CO_2 capture; 2) the ligand-free surface is beneficial to the intimate contact between neighboring QDs and to CO_2 activation on the QD surface; 3) the immobilized Ni^{2+} species on the QDs facilitate the charge separation and act as catalytic sites for CO_2 reduction. Our work provides a novel strategy to synthesize QD aerogels and offers a platform for designing various QD aerogels for photocatalytic applications. Further studies aiming to improve the photocatalytic performance of the QD aerogels by more efficient surface modification are in progress.

EXPERIMENTAL SECTION

Oil phase synthesis of colloidal CdSe QDs

The CdSe QDs with a diameter of about 3 nm were synthesized based on the reported method with some modifications.[36] Briefly, the Cd precursor of $Cd(OA)_2$ was prepared by dissolving CdO in OA and ODE (v/v, 1:5) at 250 °C. 0.0394 g of Se (0.5 mmol) was mixed with 15 mL of thus prepared Cd precursor containing 1 mmol of $Cd(OA)_2$ under vacuum at room temperature. The mixture was heated to 200 °C under nitrogen atmosphere upon vigorous stirring. After 2 min of reaction, the system was cooled to room temperature using a water bath at 10 °C. For CdSe QDs purification, the crude solution was precipitated by centrifugation at 8000 rpm for 5 min after addition of 25 mL of isopropanol and 4 mL of methanol; this procedure was followed by redispersion of the precipitate in 2 mL of dichloromethane. 2 mL of acetonitrile were used as a non-solvent for the second precipitation step. After that, the QD precipitate

was collected and dispersed in 2 mL of hexane. The final concentration of CdSe QDs solution was about 0.6 mM.

Solution-phase ligand exchange of OA-capped CdSe and their purification

The inorganic ligand exchange in the solution phase is based on the previously reported method.[37] Typically, the as-prepared QDs dispersed in hexane were mixed with NMF, followed by gradual adding the aqueous solution of $(NH_4)_2S$, while shaking the mixture or intensively stirring, if necessary. The $(NH_4)_2S$ solution was added slowly and continuously until QDs transferred from the hexane to the NMF phase. Fresh hexane was used to wash the NMF phase 3 times. For QD purification, excess acetone was used to precipitate the QDs from the NMF phase, and the resulting gelatinous precipitate was collected for subsequent gelation. In order to obtain the QD powders for the control experiments the precipitate was directly dried under vacuum at room temperature (20 ºC) overnight.

Water-promoted gelation of CdSe-S QDs and aerogel preparation

The precipitate obtained as described above was re-dispersed in 5 mL of deionized water. If the precipitate could not completely be dispersed, a small amount of a "good" solvent (NMF) was added to the system to promote complete solubilization. After keeping this aqueous solution for about 48 h in the dark, a monolithic CdSe gel was obtained. Afterwards, the as-prepared hydrogel was washed 4-5 times with a large amount of ethanol with a total duration of 2-3 days to remove possible residues. The co-catalyst Ni^{2+} was introduced by adding a certain amount of $NiCl_2$ in ethanol (2, 4, 8 or 16 µL of 0.05 M solution for the samples 1 to 4 in Figure 3a, respectively) to the CdSe-S gel and stirring for 3 min. The resulting CdSe-S/Ni gel was washed 4-5 times with excess of ethanol again. Finally, ethanol was exchanged in an autoclave with CO_2. As these washing steps can remove uncertain amount of Ni from the nanostructure, we refer in this paper to the final composition of the best performing aerogel (CdSe-S/$Ni_{(3)}$) determined

by the EDX (Figure S13). The CdSe-S/Ni aerogel was obtained by supercritical drying at 100 bar and 45 ºC with a critical point dryer 13200J0AB (Spi Supplies), equipped with a CO_2-pump.

Photocatalytic CO_2 reduction test

In a typical experiment, the QD aerogels or powders (2 mg) were attached onto a glass substrate coated with a Nafion layer (see details in **Figure S7**). The photoreactor containing the QD aerogels immobilized on the support was filled with CO_2 for 10 min to remove the air. The reactor was kept in a water bath at 25 °C. A 300 W Xe lamp (Solaredge 700, China) equipped with a 400 nm cut-off filter ($\lambda > 400$ nm, UQG Optics) was used as light source to simulate sunlight. The power density was calibrated to 100 mW cm^{-2}. The amounts of CO were determined by a gas chromatograph (GC, 7820A, Ar carrier, Agilent). The isotope-labelling experiments were performed using $^{13}CO_2$ instead of $^{12}CO_2$, and the products were analyzed using gas chromatography-mass spectrometry (GC-MS, 7890A and 5975C, Agilent). In the final photocatalytic products, neither hydrogen nor methane were detected, so we conclude that the selectivity was close to 100%.

ASSOCIATED CONTENT

Supporting Information

The Supporting Information is available free of charge on the ACS Publications website at DOI:

Additional experimental details, materials, and characterization methods. TEM image of CdSe-OA and corresponding size distribution (Figure S1). Absorption (Figure S2) and fluorescence (Figure S3) spectra of CdSe-OA QDs, CdSe-S QDs, and CdSe-S gel. Dynamic light scattering plot of various QD samples (Figure S4). HR-TEM image of CdSe-S aerogel (Figure S5). Differential TGA of various QD samples (Figure S6). Flow chart of photocatalytic reaction with

QD aerogels (Figure S7). Control experiments on photocatalytic reactions of various samples (Figure S8). Images of QDs powder and aerogel (Figure S9). The yield of O_2 on the QD aerogel (Figure S10). Control photocatalytic experiments (Figure S11). BET test results of CdSe-S/$Ni_{(3)}$ aerogel (Figure S12). XPS results of CdSe-S aerogel (Figure S13 and S14). EDX sum spectrum of CdSe-S/$Ni_{(3)}$ aerogel (Figure S15). HAADF-STEM image of the CdSe-S/$Ni_{(3)}$ aerogel and corresponding element maps (Figure S16). Absorbance of CdSe-S aerogel (Figure S17). Solid ultraviolet diffuse reflection and XPS spectrum of the CdSe-S aerogel to determine the band positions (Figure S18). A summary of the photocatalytic CO_2 reduction performance by various aerogel based photocatalysts (Table S1). Summary of nitrogen adsorption data and ligament sizes of the as-prepared aerogels (Table S2). Summary of fabrication strategies and some properties of CdSe-based QD aerogels from published results (Table S3).

AUTHOR INFORMATION

Corresponding Authors

Jin Wang − Key Laboratory of the Ministry of Education for Advanced Catalysis Materials, Zhejiang Normal University, Jinhua, Zhejiang 321004, P. R. China; orcid.org/0000-0003-4740-4304; Email: wangjin@zjnu.edu.cn

Nikolai Gaponik − Physical Chemistry, Technische Universität Dresden, Zellescher Weg 19, 01069 Dresden, Germany; orcid.org/0000-0002-8827-2881; Email: nikolai.gaponik@tu-dresden.de

Authors

Guocan Jiang − Physical Chemistry, Technische Universität Dresden, Zellescher Weg 19, 01069 Dresden, Germany;

Nuoya Li − Key Laboratory of the Ministry of Education for Advanced Catalysis Materials, Zhejiang Normal University, Jinhua, Zhejiang 321004, P. R. China;

René Hübner − Helmholtz-Zentrum Dresden-Rossendorf, Institute of Ion Beam Physics and Materials Research, Bautzner Landstrasse 400, 01328 Dresden, Germany;

Maximilian Georgi − Physical Chemistry, Technische Universität Dresden, Zellescher Weg 19, 01069 Dresden, Germany;

Bin Cai − School of Chemistry and Chemical Engineering, Shandong University, Shanda South Road 27, Jinan 250100, P.R. China;

Zhengquan Li − Key Laboratory of the Ministry of Education for Advanced Catalysis Materials, Zhejiang Normal University, Jinhua, Zhejiang 321004, P. R. China; orcid.org/0000-0002-0084-5113;

Vladimir Lesnyak − Physical Chemistry, Technische Universität Dresden, Zellescher Weg 19, 01069 Dresden, Germany; orcid.org/0000-0002-2480-8755;

Alexander Eychmüller − Physical Chemistry, Technische Universität Dresden, Zellescher Weg 19, 01069 Dresden, Germany; orcid.org/0000-0001-9926-6279;

Notes

The authors declare no competing financial interest.

ACKNOWLEDGMENTS

G. J. acknowledges the China Scholarship Council (No. 201706740088). J. W. received support from Natural Science Foundation of China (21701143). N. G. acknowledges the ERA-NET Project MINARECO funded by German Federal Ministry of Education and Research (BMBF), Grant Nr. 01DJ21009. The use of the HZDR Ion Beam Center TEM facilities and the funding of TEM Talos by the German Federal Ministry of Education of Research (BMBF), Grant No. 03SF0451, in the framework of HEMCP are acknowledged. M. G. and A. E. acknowledge the Swiss National Science Foundation (SNF) and the German Research Foundation (DFG EY 16/18-2) for financial support. We are very grateful to Prof. J. Feldmann and J. Fang for their valuable comments and discussions. We are grateful to Dr. A. Prudnikau, and Dr. W. Wei for the valuable discussions. We are also grateful to S. Goldberg and Dr. N. Weiss for TEM imaging and to L. Wang and Dr. J. Simmchen for their help in DLS measurements.

REFERENCES

[1] Inoue, T.; Fujishima, A.; Konishi, S.; Honda, K. Photoelectrocatalytic Reduction of Carbon Dioxide in Aqueous Suspensions of Semiconductor Powders. *Nature* **1979**, *277*, 637-638.

[2] White, J. L.; Baruch, M. F.; Pander, J. E.; Hu, Y.; Fortmeyer, I. C.; Park, J. E.; Zhang, T.; Liao, K.; Gu, J.; Yan, Y. et al. Light-Driven Heterogeneous Reduction of Carbon Dioxide: Photocatalysts and Photoelectrodes. *Chem. Rev.* **2015**, *115*, 12888-12935.

[3] Sakimoto, K. K.; Wong, A. B.; Yang, P. Self-Photosensitization of Nonphotosynthetic Bacteria for Solar-to-Chemical Production. *Science* **2016**, *351*, 74-77.

[4] Han, B.; Ou, X.; Deng, Z.; Song, Y.; Tian, C.; Deng, H.; Xu, Y. J.; Lin, Z. Nickel Metal–Organic Framework Monolayers for Photoreduction of Diluted CO_2 : Metal-Node-Dependent Activity and Selectivity. *Angew. Chem. Int. Ed.* **2018**, *57*, 16811-16815.

[5] Wu, H. L.; Li, X. B.; Tung, C. H.; Wu, L. Z. Semiconductor Quantum Dots: An Emerging Candidate for CO_2 Photoreduction. *Adv. Mater.* **2019**, *31*, 1900709.

[6] Chang, X. X.; Wang, T.; Gong, J. L. CO_2 Photo-Reduction: Insights into CO_2 Activation and Reaction on Surfaces of Photocatalysts. *Energy Environ. Sci.* **2016**, *9*, 2177-2196.

[7] Li, Z.-J.; Wang, J.-J.; Li, X.-B.; Fan, X.-B.; Meng, Q.-Y.; Feng, K.; Chen, B.; Tung, C.-H.; Wu, L.-Z. An Exceptional Artificial Photocatalyst, Nih-CdSe/CdS Core/Shell Hybrid, Made In Situ from CdSe Quantum Dots and Nickel Salts for Efficient Hydrogen Evolution. *Adv. Mater.* **2013**, *25*, 6613-6618.

[8] Yu, X.; Shavel, A.; An, X.; Luo, Z.; Ibáñez, M.; Cabot, A. Cu_2ZnSnS_4-Pt and Cu_2ZnSnS_4-Au Heterostructured Nanoparticles for Photocatalytic Water Splitting and Pollutant Degradation. *J. Am. Chem. Soc.* **2014**, *136*, 9236-9239.

[9] Kuehnel, M. F.; Orchard, K. L.; Dalle, K. E.; Reisner, E. Selective Photocatalytic CO_2 Reduction in Water through Anchoring of a Molecular Ni Catalyst on CdS Nanocrystals. *J. Am. Chem. Soc.* **2017**, *139*, 7217-7223.

[10] Lian, S. C.; Kodaimati, M. S.; Dolzhnikov, D. S.; Calzada, R.; Weiss, E. A. Powering a CO_2 Reduction Catalyst with Visible Light through Multiple Sub-Picosecond Electron Transfers from a Quantum Dot. *J. Am. Chem. Soc.* **2017**, *139*, 8931-8938.

[11] Li, X. B.; Tung, C. H.; Wu, L. Z. Semiconducting Quantum Dots for Artificial Photosynthesis. *Nat. Rev. Chem.* **2018**, *2*, 160-173.

[12] Stolarczyk, J. K.; Bhattacharyya, S.; Polavarapu, L.; Feldmann, J. Challenges and Prospects in Solar Water Splitting and CO_2 Reduction with Inorganic and Hybrid Nanostructures. *ACS Catal.* **2018**, *8*, 3602-3635.

[13] Wang, J.; Xia, T.; Wang, L.; Zheng, X.; Qi, Z.; Gao, C.; Zhu, J.; Li, Z.; Xu, H.; Xiong, Y. Enabling Visible-Light-Driven Selective CO_2 Reduction by Doping Quantum Dots: Trapping Electrons and Suppressing H_2 Evolution. *Angew. Chem. Int. Ed.* **2018**, *57*, 16447-16451.

[14] Fan, X.-B.; Yu, S.; Wang, X.; Li, Z.-J.; Zhan, F.; Li, J.-X.; Gao, Y.-J.; Xia, A.-D.; Tao, Y.; Li, X.-B. et al. Susceptible Surface Sulfide Regulates Catalytic Activity of CdSe Quantum Dots for Hydrogen Photogeneration. *Adv. Mater.* **2019**, *31*, 1804872.

[15] Chen, Z.; Hu, Y.; Wang, J.; Shen, Q.; Zhang, Y.; Ding, C.; Bai, Y.; Jiang, G.; Li, Z.; Gaponik, N. Boosting Photocatalytic CO_2 Reduction on $CsPbBr_3$ Perovskite Nanocrystals by Immobilizing Metal Complexes. *Chem. Mater.* **2020**, *32*, 1517-1525.

[16] Xia, W.; Wu, J.; Hu, J. C.; Sun, S. S.; Li, M. D.; Liu, H. F.; Lan, M. H.; Wang, F. Highly Efficient Photocatalytic Conversion of CO_2 to CO Catalyzed by Surface-Ligand-Removed and Cd-Rich CdSe Quantum Dots. *ChemSusChem* **2019**, *12*, 4617-4622.

[17] Manzi, A.; Simon, T.; Sonnleitner, C.; Doblinger, M.; Wyrwich, R.; Stern, O.; Stolarczyk, J. K.; Feldmann, J. Light-Induced Cation Exchange for Copper Sulfide Based CO_2 Reduction. *J. Am. Chem. Soc.* **2015**, *137*, 14007-14010.
[18] Chang, C. M.; Orchard, K. L.; Martindale, B. C. M.; Reisner, E. Ligand Removal from CdS Quantum Dots for Enhanced Photocatalytic H_2 Generation in pH Neutral Water. *J. Mater. Chem. A* **2016**, *4*, 2856-2862.
[19] Simon, T.; Bouchonville, N.; Berr, M. J.; Vaneski, A.; Adrovic, A.; Volbers, D.; Wyrwich, R.; Doblinger, M.; Susha, A. S.; Rogach, A. L. et al. Redox Shuttle Mechanism Enhances Photocatalytic H_2 Generation on Ni-Decorated CdS Nanorods. *Nat. Mater.* **2014**, *13*, 1013-1018.
[20] Wan, W.; Zhang, R.; Ma, M.; Zhou, Y. Monolithic Aerogel Photocatalysts: A Review. *J. Mater. Chem. A* **2018**, *6*, 754-775.
[21] Xiao, J. D.; Jiang, H. L. Metal-Organic Frameworks for Photocatalysis and Photothermal Catalysis. *Acc. Chem. Res.* **2019**, *52*, 356-366.
[22] Wang, H.; Wang, H.; Wang, Z. W.; Tang, L.; Zeng, G. M.; Xu, P.; Chen, M.; Xiong, T.; Zhou, C. Y.; Li, X. Y. et al. Covalent Organic Framework Photocatalysts: Structures and Applications. *Chem. Soc. Rev.* **2020**, *49*, 4135-4165.
[23] Luna, A. L.; Matter, F.; Schreck, M.; Wohlwend, J.; Tervoort, E.; Colbeau-Justin, C.; Niederberger, M. Monolithic Metal-Containing TiO_2 Aerogels Assembled from Crystalline Preformed Nanoparticles as Efficient Photocatalysts for H_2 Generation. *Appl. Catal. B* **2020**, *267*, 118660.
[24] Schreck, M.; Niederberger, M. Photocatalytic Gas Phase Reactions. *Chem. Mater.* **2019**, *31*, 597-618.
[25] Berestok, T.; Guardia, P.; Portals, J. B.; Estradé, S.; Llorca, J.; Peiró, F.; Cabot, A.; Brock, S. L. Surface Chemistry and Nano-/Microstructure Engineering on Photocatalytic In_2S_3 Nanocrystals. *Langmuir* **2018**, *34*, 6470-6479.
[26] Rechberger, F.; Niederberger, M. Translucent Nanoparticle-Based Aerogel Monoliths as 3-Dimensional Photocatalysts for the Selective Photoreduction of CO_2 to Methanol in a Continuous Flow Reactor. *Mater. Horiz.* **2017**, *4*, 1115-1121.
[27] Korala, L.; Germain, J. R.; Chen, E.; Pala, I. R.; Li, D.; Brock, S. L. CdS Aerogels as Efficient Photocatalysts for Degradation of Organic Dyes under Visible Light Irradiation. *Inorg. Chem. Front.* **2017**, *4*, 1451-1457.
[28] Bi, Q. Q.; Wang, J. W.; Lv, J. X.; Wang, J.; Zhang, W.; Lu, T. B. Selective Photocatalytic CO_2 Reduction in Water by Electrostatic Assembly of CdS Nanocrystals with a Dinuclear Cobalt Catalyst. *ACS Catal.* **2018**, *8*, 11815-11821.
[29] Zambo, D.; Schlosser, A.; Rusch, P.; Luebkemann, F.; Koch, J.; Pfnuer, H.; Bigall, N. C. A Versatile Route to Assemble Semiconductor Nanoparticles into Functional Aerogels by Means of Trivalent Cations. *Small* **2020**, *16*, 1906934.
[30] Sayevich, V.; Cai, B.; Benad, A.; Haubold, D.; Sonntag, L.; Gaponik, N.; Lesnyak, V.; Eychmüller, A. 3D Assembly of All-Inorganic Colloidal Nanocrystals into Gels and Aerogels. *Angew. Chem. Int. Ed.* **2016**, *55*, 6334-6338.
[31] Naskar, S.; Miethe, J. F.; Sánchez-Paradinas, S.; Schmidt, N.; Kanthasamy, K.; Behrens, P.; Pfnür, H.; Bigall, N. C. Photoluminescent Aerogels from Quantum Wells. *Chem. Mater.* **2016**, *28*, 2089-2099.
[32] Singh, A.; Lindquist, B. A.; Ong, G. K.; Jadrich, R. B.; Singh, A.; Ha, H.; Ellison, C. J.; Truskett, T. M.; Milliron, D. J. Linking Semiconductor Nanocrystals into Gel Networks through All-Inorganic Bridges. *Angew. Chem. Int. Ed.* **2015**, *54*, 14840-14844.

[33] Lesnyak, V.; Voitekhovich, S. V.; Gaponik, P. N.; Gaponik, N.; Eychmüller, A. CdTe Nanocrystals Capped with a Tetrazolyl Analogue of Thioglycolic Acid: Aqueous Synthesis, Characterization, and Metal-Assisted Assembly. *ACS Nano* **2010**, *4*, 4090-4096.
[34] Yu, H.; Bellair, R.; Kannan, R. M.; Brock, S. L. Engineering Strength, Porosity, and Emission Intensity of Nanostructured CdSe Networks by Altering the Building-Block Shape. *J. Am. Chem. Soc.* **2008**, *130*, 5054-5055.
[35] Mohanan, J. L.; Arachchige, I. U.; Brock, S. L. Porous Semiconductor Chalcogenide Aerogels. *Science* **2005**, *307*, 397-400.
[36] Pu, C.; Zhou, J.; Lai, R.; Niu, Y.; Nan, W.; Peng, X. Highly Reactive, Flexible Yet Green Se Precursor for Metal Selenide Nanocrystals: Se-Octadecene Suspension (Se-SUS). *Nano Res.* **2013**, *6*, 652-670.
[37] Nag, A.; Kovalenko, M. V.; Lee, J.-S.; Liu, W.; Spokoyny, B.; Talapin, D. V. Metal-free Inorganic Ligands for Colloidal Nanocrystals: S^{2-}, HS^{-}, Se^{2-}, HSe^{-}, Te^{2-}, HTe^{-}, TeS_3^{2-}, OH^{-}, and NH_2^{-} as Surface Ligands. *J. Am. Chem. Soc.* **2011**, *133*, 10612-10620.
[38] Chakrapani, V.; Baker, D.; Kamat, P. V. Understanding the Role of the Sulfide Redox Couple (S^{2-}/S_n^{2-})) in Quantum Dot-Sensitized Solar Cells. *J. Am. Chem. Soc.* **2011**, *133*, 9607-9615.
[39] Wei, H. H.-Y.; Evans, C. M.; Swartz, B. D.; Neukirch, A. J.; Young, J.; Prezhdo, O. V.; Krauss, T. D. Colloidal Semiconductor Quantum Dots with Tunable Surface Composition. *Nano Lett.* **2012**, *12*, 4465-4471.
[40] Du, R.; Hu, Y.; Hubner, R.; Joswig, J. O.; Fan, X. L.; Schneider, K.; Eychmüller, A. Specific Ion Effects Directed Noble Metal Aerogels: Versatile Manipulation for Electrocatalysis and Beyond. *Sci. Adv.* **2019**, *5*, eaaw4590.
[41] Gaponik, N.; Wolf, A.; Marx, R.; Lesnyak, V.; Schilling, K.; Eychmüeller, A. Three-Dimensional Self-Assembly of Thiol-Capped CdTe Nanocrystals: Gels and Aerogels as Building Blocks for Nanotechnology. *Adv. Mater.* **2008**, *20*, 4257-4262.
[42] Du, R.; Fan, X.; Jin, X.; Hübner, R.; Hu, Y.; Eychmüller, A. Emerging Noble Metal Aerogels: State of the Art and a Look Forward. *Matter* **2019**, *1*, 39-56.
[43] Cai, B.; Sayevich, V.; Gaponik, N.; Eychmüller, A. Emerging Hierarchical Aerogels: Self-Assembly of Metal and Semiconductor Nanocrystals. *Adv. Mater.* **2018**, *30*, 1707518.
[44] Fan, X.; Cai, B.; Du, R.; Hübner, R.; Georgi, M.; Jiang, G.; Li, L.; Samadi Khoshkhoo, M.; Sun, H.; Eychmüller, A. Ligand-Exchange-Mediated Fabrication of Gold Aerogels Containing Different Au(I) Content with Peroxidase-like Behavior. *Chem. Mater.* **2019**, *31*, 10094-10099.
[45] Zhang, H.; Wang, D. Controlling the Growth of Charged-Nanoparticle Chains through Interparticle Electrostatic Repulsion. *Angew. Chem. Int. Ed.* **2008**, *47*, 3984-3987.
[46] Pala, I. R.; Arachchige, I. U.; Georgiev, D. G.; Brock, S. L. Reversible Gelation of II-VI Nanocrystals: The Nature of Interparticle Bonding and the Origin of Nanocrystal Photochemical Instability. *Angew. Chem. Int. Ed.* **2010**, *49*, 3661-3665.
[47] Sherman, Z. M.; Green, A. M.; Howard, M. P.; Anslyn, E. V.; Truskett, T. M.; Milliron, D. J. Colloidal Nanocrystal Gels from Thermodynamic Principles. *Acc. Chem. Res.* **2021**, *54*, 798-807.
[48] Ziegler, C.; Wolf, A.; Liu, W.; Herrmann, A. K.; Gaponik, N.; Eychmüller, A. Modern Inorganic Aerogels. *Angew. Chem. Int. Ed.* **2017**, *56*, 13200-13221.
[49] Naskar, S.; Freytag, A.; Deutsch, J.; Wendt, N.; Behrens, P.; Köckritz, A.; Bigall, N. C. Porous Aerogels from Shape-Controlled Metal Nanoparticles Directly from Nonpolar Colloidal Solution. *Chem. Mater.* **2017**, *29*, 9208-9217.
[50] Li, Z.-J.; Fan, X.-B.; Li, X.-B.; Li, J.-X.; Zhan, F.; Tao, Y.; Zhang, X.; Kong, Q.-Y.; Zhao, N.-J.; Zhang, J.-P. et al. Direct Synthesis of All-Inorganic Heterostructured CdSe/CdS QDs in Aqueous Solution for Improved Photocatalytic Hydrogen Generation. *J. Mater. Chem. A* **2017**, *5*, 10365-10373.

[51] Pearson, R. G. Hard and Soft Acids and Bases. *J. Am. Chem. Soc.* **1963**, *85*, 3533-3539.
[52] Yang, H. J.; Luo, M.; Chen, X. T.; Zhao, X.; Lin, J.; Hu, D. D.; Li, D. S.; Bu, X. H.; Feng, P. Y.; Wu, T. Cation-Exchanged Zeolitic Chalcogenides for CO_2 Adsorption. *Inorg. Chem.* **2017**, *56*, 14999-15005.
[53] Sasan, K.; Lin, Q. P.; Mao, C. Y.; Feng, P. Y. Open Framework Metal Chalcogenides as Efficient Photocatalysts for Reduction of CO_2 into Renewable Hydrocarbon Fuel. *Nanoscale* **2016**, *8*, 10913-10916.
[54] Hendel, T.; Lesnyak, V.; Kuhn, L.; Herrmann, A. K.; Bigall, N. C.; Borchardt, L.; Kaskel, S.; Gaponik, N.; Eychmüller, A. Mixed Aerogels from Au and CdTe Nanoparticles. *Adv. Funct. Mater.* **2013**, *23*, 1903-1911.
[55] Li, X. B.; Tung, C. H.; Wu, L. Z. Quantum Dot Assembly for Light-Driven Multielectron Redox Reactions, such as Hydrogen Evolution and CO_2 Reduction. *Angew. Chem. Int. Ed.* **2019**, *58*, 10804-10811.
[56] Cheng, C.; He, B. W.; Fan, J. J.; Cheng, B.; Cao, S. W.; Yu, J. G. An Inorganic/Organic S-Scheme Heterojunction H_2-Production Photocatalyst and its Charge Transfer Mechanism. *Adv. Mater.* **2021**, *33*, 2100317.

Table of Contents Graphic